

Self assembly of microparticles in stable ring structures in an optical trap

Arijit Haldar, Sambit Bikas Pal, Basudev Roy, and Ayan Banerjee*

Department of Physical Sciences, IISER-Kolkata, Mohanpur 741252, India

S. Dutta Gupta

School of Physics, University of Hyderabad, Hyderabad 500046, India

(Dated: May 29, 2022)

Abstract

Micro-particle self assembly under the influence of optical forces produced by higher order optical beams or by projection of a hologram into the trapping volume is well known. In this paper, we report the spontaneous formation of a ring of identical microspheres (each with diameter $1.1 \mu\text{m}$) in conventional single beam optical tweezers having standing wave geometry with the sample chamber consisting of a cover slip and glass slide, and a usual TEM_{00} Gaussian beam. The effects of different experimental parameters on the ring formation are studied extensively. The experimental observations are backed by theoretical simulations based on a plane wave decomposition of the forward and backward propagating Gaussian beams. The ring patterns are shown to be caused due to geometrical aberrations produced by focusing the Gaussian beam using a high numerical aperture microscope objective into stratified media. It is found that the thickness of the stratified media and the standing wave geometry itself play a critical role in formation of stable ring structures. These structures could be used in the study of optical binding, thermally activated transitions, as well as biological interactions between cells in an optical trap.

PACS numbers: 42.50.Wk, 87.80.Cc, 42.25.-p:

* ayan@iiserkol.ac.in

I. INTRODUCTION

Optical tweezers offer the possibilities of applying controlled forces of extremely small magnitude (pN-fN) to trap and manipulate mesoscopic particles - as a result of which they have widespread applications in physics [1–3] and biology [4–7]. For relatively large particles (size between few to several tens of microns), it is easy to trap single particles at the trap center, while for nanoparticles, clusters assemble with time in the central region [8]. Micro-particle self-assembly is interesting since it provides an insight into the dynamics of particles in a well-understood force environment, interactions between particles (such as cells [9]), and processes where particles themselves modify the force environment as is manifested in optical binding [10]. The most widely used way of creating microparticle assembly in optical traps is by modifying the trapping beam to include higher order axial modes (TEM_{10} , TEM_{11} , etc), vortex beams (Laguerre-Gaussian modes), as well as interference patterns by using a spatial light modulator [11]. Micro-particle assembly has also been observed due to surface tension effects between adjacent particles. It has been shown that multiple polystyrene micro-spheres can coalesce together inside a single trap, to form highly symmetric closed pack structures [12]. Another effect that has shown to form specifically ring-like structures at the laser focus is the phenomenon of thermo-capillarity [13], where the high power of the trapping laser causes convection currents at the focal spot, resulting in the micro-spheres being displaced away from the center. When an equilibrium is reached between the trapping force and the forces exerted from the convection currents, a ring like structure forms. Thermo-capillary effects are highly sensitive to the change in the power of the trapping beam, with the ring diameter increasing proportionally with the power until the chain of particles breaks at certain powers.

In this paper, we report the stable trapping of polystyrene beads of diameter 1100 nm in ring structures around the centre of the optical trap where we use a single pure Gaussian beam (TEM_{00}) for trapping the particles. The diameter of the rings can be varied between $\sim 3 - 5 \mu\text{m}$ by changing the z-focus of the trapping microscope, with the number of trapped particles in a closed ring varying between 9-15. Our sample chamber consisted of a cover slip and a slide, with the sample (polystyrene beads dispersed in water) sandwiched between. This particular configuration was critical to the formation of rings, which were not seen in the absence of a top slide. Our beam was checked to be a pure Gaussian TEM_{00} by

a standard beam profile measurement using a sharp edge mounted on a translation stage - in addition, to remove any uncertainty about higher order axial modes being contained in the beam, we coupled our trapping laser into a single mode fiber. The ring formation remained unaffected by this step in the experimental procedure, which thus implied that the effect was not due to such higher order modes in the trapping beam itself. Also, the closed pack structures reported in Ref. [12] are not dependent on the presence of a top slide, and typically occur when one of the beads is in *contact* with a surface - both circumstances being very different from our observations. Such dependence is not observed in our experiments. In addition, the fact that we do not observe any dependence of ring radius on the power of the laser beam indicates that thermo-capillary effects [13] are not involved in the formation of particle rings.

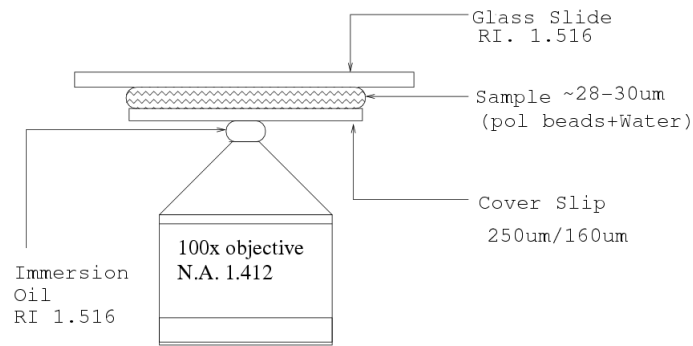
It therefore appears that the phenomenon we observe has not been reported in literature. We thus perform theoretical simulations to understand the structure of the electric field inside the sample chamber that could support the formation of such stable ring structures. The structure of the paper is as follows. In Section II, we discuss the experimental conditions for obtaining the ring structure in detail. In Section III, we lay out the theoretical model we have used to find the field in both radial and axial directions inside the sample chamber. Section IV describes the simulations performed and a thorough analysis of the simulation results to explain our experimental findings. We end the paper with a few possible applications of such ring formation and future work that is planned in Section V.

II. EXPERIMENT AND OBSERVATIONS

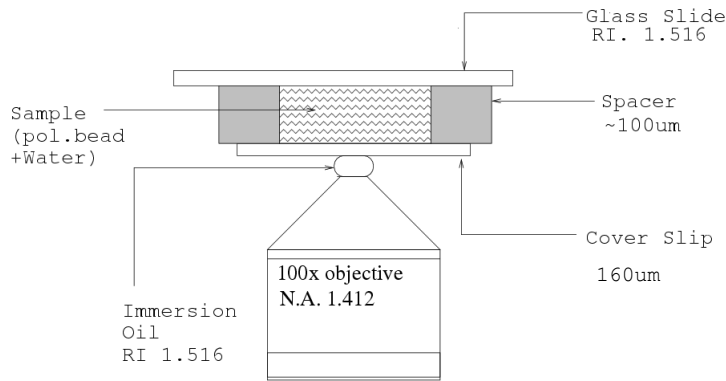
The setup consisted of an inverted microscope with a high power IR laser (Lasever LSR1064ML, 1064 nm, max power 800 mW) fed into the microscope (Carl Zeiss Axiovert.A1) back port, so that the laser beam was focused tightly on the sample using a high numerical aperture objective (Zeiss 100X, oil immersion, plan apochromat, 1.41 NA, infinity corrected) lens arrangement. The typical specified working distance of this objective is 170 μm - however, we observed that we could focus into our sample chamber at distances around 300 μm from the exit pupil of the objective. This was verified by using the 250 μm coverslip and putting two fiducial marks - one on the top surface of the coverslip, and the other on the bottom surface of the slide. We observed that when we increased the sample thickness to

more than $40\ \mu\text{m}$, the fiducial mark on the slide could no longer be imaged. The sample consists of a dilute solution of monodispersed polystyrene micro-spheres (mean diameter $1.1\ \mu\text{m}$, Sigma Aldrich LB11) in distilled water (dilution 1:10000) placed in a sample chamber consisting of a glass slide and cover slip. The cover slips we used were of two types: 1) made of English glass (RI = 1.512 at 1064 nm) having thickness $160\ \mu\text{m}$, and 2) made of a polymer (Sigma Aldrich Hybrid Cover-slips, Part no. Z365912-100EA) having refractive index of 1.575 (at 1064 nm) and thickness of $250\ \mu\text{m}$. The refractive index of the Type 2 cover slips was measured using a commercial refractometer (Prism Coupler - Metricon Model-2010). Therefore, only in the case of the $250\ \mu\text{m}$ coverslip was there a significant refractive index mismatch between the cover slip and immersion oil. We used two methods of preparing the sample chamber - a) Configuration 1, where we put the sample on the cover slip and directly attached the cover slip on top so that there was a thin film of micro-sphere solution between slide and cover slip, and b) Configuration 2, where we used a spacer of thickness around $100\ \mu\text{m}$ consisting of double-sided sticky tape between the cover slip and slide. Note that this configuration could not be used for $250\ \mu\text{m}$ coverslips due to focusing problems of the microscope objective. The arrangements are shown in Fig. 1.

When we performed the experiment using configuration 1 with $250\ \mu\text{m}$ thick cover slips, for a sample chamber thickness of around $30\ \mu\text{m}$ (distance between slide and cover slip), we observed a spontaneous formation of ring-like structures of microparticles as shown in Fig. 2. The particles were allowed to accumulate gradually, and soon formed closed ring structures after slight manipulation of the microscope focus. If the trap was switched off, the particles diffused away, only to reassemble almost instantaneously in the same ring structure after the trap was switched on again. There was occasionally a particle trapped in the center, but the most likely region of trapping was in the ring some distance away from the center (also the focus of the microscope). The radius of the ring could be varied as well by changing the focus of the microscope. We could change the diameter of the rings between a minimum of around $3\ \mu\text{m}$ to $5\ \mu\text{m}$. The diameter was obtained by noting the circumference of the ring, which to close approximation was the product of the number of microspheres (that varied between 9 to 15) in a complete ring and the individual microsphere diameter ($1.1\ \mu\text{m}$). The ring diameter could then be obtained by dividing the circumference by π . The diameter was also verified by analyzing the image of a given ring in standard softwares such as Canvas or Adobe Illustrator.



(a) Configuration 1: Sample chamber without spacer



(b) Configuration 2: Sample chamber with spacer

FIG. 1: Two types of sample chamber configurations used in the experiment

This observation clearly contradicts the normal model of microsphere trapping by well shaped Gaussian beams. At best, simultaneous trapping of multiple particles would have led to clumping of particles at the trap center and not the assembly of particles in an axis-symmetric ring. It seems most likely that the field distribution in that area is quite different from that of the normal Gaussian beam. Furthermore the ring like structures showed the following attributes which implied that their formation was due to an interplay of optical

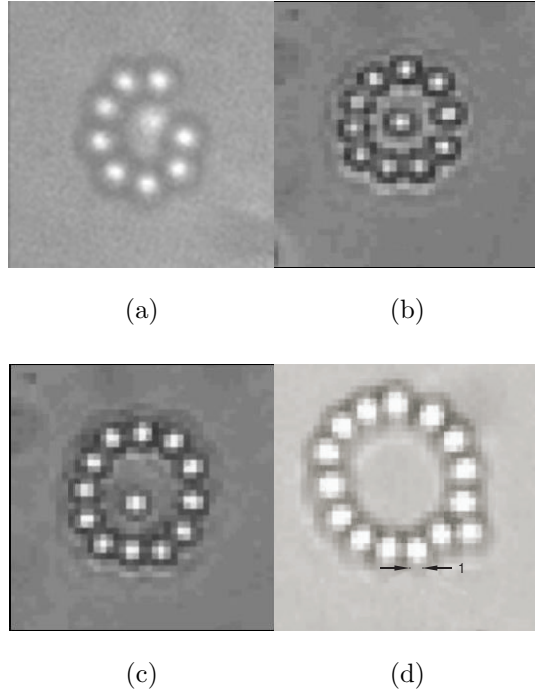


FIG. 2: Radial Pattern formation with $250 \mu\text{m}$ coverslips with (a) 8, (b) 10, (c) 12, and (d) 14 particles in the ring. (a), (b), and (c) could possibly accommodate one more particle.

Dimensions are in microns.

effects.

- Under normal imaging conditions (i.e. when the camera is attached to the side port of the microscope), the rings form only with sample loading Configuration 1 with $250 \mu\text{m}$ coverslips. Any deviation from the mentioned arrangement destroys the formation of rings and the micro-spheres clump up at the center of the trap. Rings are not observed in Configuration 2, or even if we increase the water volume in Configuration 1, such that the thickness of the water meniscus increases to around $50 \mu\text{m}$.
- Rings are also observed for $160 \mu\text{m}$ coverslips with Configuration 1, when imaging is done *outside* the microscope. This indicates that the plane at which rings form for the $250 \mu\text{m}$ case is considerably different for the $160 \mu\text{m}$ case, so much so that external optics have to be used to bring the plane into focus.
- The diameter of a ring can be controlled by changing the focus of the objective lens, which means we do have axial trapping. Changing the distance of the objective lens

from the sample moves the focus up or down and this changes the diameter of the ring. We have also reduced the input beam diameter from 5 mm (that overfills the objective) to around 2 mm, and observed a corresponding reduction of the ring diameter.

- As we move the objective along the z-axis in a clockwise direction (i.e. in the direction of the trapping beam), we first observe trapping at the focus of the laser beam. As we move further in, we observe a ring formation of particles, i.e. they are no longer trapped at the center (focus) of the beam. This implies that trapping at the focus is closer to the cover-slip or near the center of the trap, whereas the ring formation is almost certainly closer to the top surface, i.e. the slide. In fact, the rings formed about 5-6 μm below top glass slide, or around 24 μm inside the sample chamber for a sample thickness of 30 μm . This calibration was performed by the z-axis vernier of the microscope (least count 1 μm).
- We do not observe any ring formation without the presence of a top surface, i.e. in the absence of a glass slide on top of the cover-slip.
- The ring formation is virtually independent of power. The trapping power is 160 mW in the trap (from a total laser power of around 800 mW). We have seen ring formation even at around 50 mW total laser power (which means around 16 mW at the trap). We have seen no change in ring formation when we:
 - obtain the ring at high power and subsequently reduce the power, or
 - start at low power itself.
- To find the stiffness of our optical trap, we performed measurements of the corner frequency of a single bead trapped in the laser focus, as well as that of a bead trapped in the ring by the power spectrum method [14]. The corner frequency is also a direct measure of the trapping force [15], and we obtain values of around 165 Hz for a single trapped bead at the beam focus for a glass coverslip, and around 18 Hz for a bead trapped in a ring for a polymer cover slip. Since all other conditions remain the same, the ratio between the trapping forces thus comes to be around 9.2.

From the findings above, it is apparent that we need to understand the electric field between the coverslip and the slide in Configuration 1 for 250 and 160 μm cover slips. An

experimental study would principally comprise of imaging the field, and in our attempts at directly imaging the back-scatter from the sample chamber, we have observed a fringe-like structure in the trapping plane, where particles seem to accumulate predominantly in the first maxima. However, it is important to note that the imaged field will be a superposition of the fields at all planes in the sample, containing both scattered fields from the micro-sphere, and reflected fields from the different chamber surfaces. A confocal imaging of the plane where the micro-spheres are trapped could be performed in principle, but even that would not allow one to separate out the scattered and reflected constituents of the field. Furthermore, controlled changes of experimental parameters, such as variation of cover slip thickness is ruled out due to lack of commercial availability. It is thus obvious that a theoretical model of our system is needed.

III. THEORETICAL MODELING

It is clear that the total field in our sample chamber will be a superposition of forward and backward propagating waves with respect to the sample chamber. What really complicates the problem is the radial variation of the beam that arises from its transverse distribution. While there exists literature on the axial distribution of the light field [16, 17], the radial distribution has not been adequately investigated in optical traps. We use a similar model as in Refs. 16 and 17, but extend it in the radial direction to find the field distribution inside the sample chamber under various circumstances. Accordingly, we use the well known Angular Spectrum Method (also referred to as vectorial Debye diffraction theory or Debye integral) [18] to calculate the electric field distribution for high numerical aperture optics in stratified media without the use of the paraxial approximation. The approach basically consists of using proper boundary conditions that are necessary to propagate electric fields across multiple interfaces between layered media incorporating the effects of high numerical aperture lenses on refracted fields. We finally use the vectorial electric field distribution integrals for the forward and backward traveling fields inside a particular media with the appropriate Fresnel coefficients for multiple interfaces.

The field at the focus of an aplanatic lens (which, for our case, would be the microscope

objective) is given by the angular spectrum integral [18]

$$\vec{E}(\rho, \psi, z) = i \frac{k f e^{-ikf}}{2\pi} \int_0^{\theta_{max}} \int_0^{2\pi} \vec{E}_{\infty}(\theta, \phi) e^{ikz \cos \theta} e^{ik\rho \sin \theta \cos(\phi-\psi)} \sin(\theta) d\theta d\phi \quad (1)$$

where r is set to f the focal length of the lens, since the integration is over the spherical wavefront of radius f . The limit for the θ integral is set by the numerical aperture of the microscope objective. The coordinate system used is shown in Fig. 3. Note that the electric field is calculated in cylindrical coordinates, while the k vectors are represented in spherical polar coordinates. The choice of cylindrical coordinates for the electric field makes it convenient to track the polarization of the light beam at the output of a high numerical aperture objective, where it is completely modified from the incident polarization [19]. We have assumed the incident polarization to be in the x direction in cartesian coordinates. The final polarization $E_{\infty}(\rho, \phi)$ is related to the incident polarization $E_{inc}(\rho', \phi')$ by

$$\vec{E}_{\infty}(\rho', \phi') = E_{inc}(\rho', \phi') \left(\cos \phi' \hat{\theta} - \sin \phi' \hat{\phi}' \right) \quad (2)$$

Using the cartesian form of the unit vectors $\hat{\theta}$ and $\hat{\phi}$, we obtain

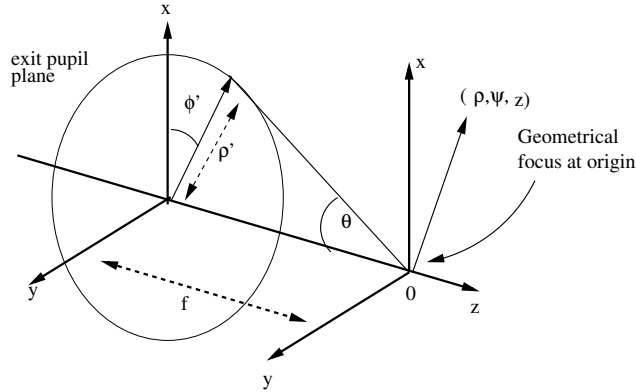


FIG. 3: Coordinate system for the problem

$$\begin{aligned} \hat{\theta} &= \cos \theta \cos \phi' \hat{i} + \cos \theta \sin \phi' \hat{j} + \sin \theta \hat{k} \\ \hat{\phi} &= \hat{\phi}' = -\sin \phi' \hat{i} + \cos \phi' \hat{j} \end{aligned} \quad (3)$$

so that the final polarization can be written as

$$\vec{E}_{\infty}(\theta, \phi) = \frac{E_{inc}(\theta, \phi)}{2} \begin{bmatrix} \{(1 + \cos \theta) - (1 - \cos \theta) \cos(2\phi)\} \hat{i} \\ \{-(1 - \cos \theta) \sin(2\phi)\} \hat{j} \\ \{-2 \cos \phi \sin \theta\} \hat{k} \end{bmatrix} \sqrt{\cos \theta} \quad (4)$$

where the $\sqrt{\cos\theta}$ term came from the apodization function for an aplanatic lens [16]. Now, in general, \vec{E}_{inc} can have a phase curvature. However, to keep things simple, we assume that it hits the entrance pupil of the lens with a planar phase front perpendicular to the optical axis. Also if the beam is a fundamental Gaussian, then the intensity distribution is independent of ϕ , and equation 1 can be written as

$$\vec{E}(\rho, \psi, z) = \frac{ikf}{2} e^{-ikf} \begin{bmatrix} \{I_0 + I_2 \cos(2\psi)\} \hat{i} \\ \{I_2 \sin(2\psi)\} \hat{j} \\ \{i2I_1 \cos(\psi)\} \hat{k} \end{bmatrix}$$

where,

$$I_0 = \int_0^{\theta_{max}} E_{inc}(\theta) \sqrt{\cos\theta} (1 + \cos\theta) J_0(k\rho \sin\theta) e^{ikz \cos\theta} \sin\theta d\theta \quad (5)$$

$$I_1 = \int_0^{\theta_{max}} E_{inc}(\theta) \sqrt{\cos\theta} J_1(k\rho \sin\theta) e^{ikz \cos\theta} \sin^2\theta d\theta \quad (6)$$

$$I_2 = \int_0^{\theta_{max}} E_{inc}(\theta) \sqrt{\cos\theta} (1 - \cos\theta) J_2(k\rho \sin\theta) e^{ikz \cos\theta} \sin\theta d\theta \quad (7)$$

where the ϕ integrals have been carried out and related to Bessel functions J_n .

Thus, with the vector field equations at the focus of an aplanatic lens known, we now consider the aplanatic lens placed in front of a multi-layered media, with the focused light beam propagating through n different dielectric interfaces as shown in Fig. 4. The integrals

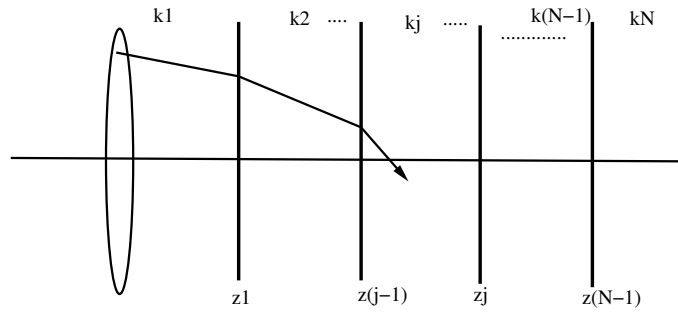


FIG. 4: Aplanatic lens focusing inside the j th medium in a N layered stratified media

for finding the forward and backward traveling fields inside the j th media can then be

written down directly

$$\vec{E}_t(\rho, \psi, z) = \frac{ikf}{2} e^{-ikf} \begin{bmatrix} \{I_0^t + I_2^t \cos(2\psi)\} \hat{i} \\ \{I_2^t \sin(2\psi)\} \hat{j} \\ \{i2 I_1^t \cos(\psi)\} \hat{k} \end{bmatrix}$$

where,

$$\begin{aligned} I_0^t &= \int_0^{\min(\theta_{max}, \theta_c)} E_{inc}(\theta) \sqrt{\cos \theta} (T_s^{(1,j)} + T_p^{(1,j)} \cos \theta_j) J_0(k_1 \rho \sin \theta) e^{ik_j z \cos \theta_j} \sin(\theta) d\theta \\ I_1^t &= \int_0^{\min(\theta_{max}, \theta_c)} E_{inc}(\theta) \sqrt{\cos \theta} T_p^{(1,j)} \sin \theta_j J_1(k_1 \rho \sin \theta) e^{ik_j z \cos \theta_j} \sin \theta d\theta \\ I_2^t &= \int_0^{\min(\theta_{max}, \theta_c)} E_{inc}(\theta) \sqrt{\cos \theta} (T_s^{(1,j)} - T_p^{(1,j)} \cos \theta_j) J_2(k_1 \rho \sin \theta) e^{ik_j z \cos \theta_j} \sin \theta d\theta \end{aligned} \quad (8)$$

where we use the Fresnel coefficients T_s and T_p for multiple interfaces. These are related to the Fresnel coefficients t_i and r_i ($i = s, p$ polarizations) for a single interface by

$$\begin{aligned} T_i^{(n-1, n+1)} &= \sum_{n=1}^{j-1} \left(\frac{t_i^{(n-1, n)} t_i^{(n, n+1)} e^{i\beta}}{1 + r_i^{(n-1, n)} r_i^{(n, n+1)} e^{i2\beta}} \right) \\ &\quad e^{i(z_{n-1} k_{n-1} \cos \theta_{n-1} - z_n k_{n+1} \cos \theta_{n+1})} \\ R_i^{(n-1, n+1)} &= \sum_{n=1}^{j-1} \left(\frac{r_i^{(n-1, n)} + r_i^{(n, n+1)} e^{i2\beta}}{1 + r_i^{(n-1, n)} r_i^{(n, n+1)} e^{i2\beta}} \right) \\ &\quad e^{i2z_{n-1} k_{n-1} \cos \theta_{n-1}} \end{aligned} \quad (9)$$

where,

$$\beta = (z_n - z_{n-1}) k_n \cos \theta_n \quad (10)$$

. It is interesting to note that an aberration term is also present in Eq. 8 hidden inside the transmission coefficients, and is given by

$$\Phi(\theta) = \sum_{n=1}^{j-1} z_n (k_n \cos \theta_n - k_{n+1} \cos \theta_{n+1}) \quad (11)$$

where z_n is the location of the n th interface. This is basically the well-known spherical aberration term that appears due to refractive index mismatch at different dielectric interfaces.

The reflected field integral inside the j th medium is also calculated similarly and is given by

$$\vec{E}(\rho, \psi, z) = \frac{ikf}{2} e^{-ikf} \begin{bmatrix} \{I_0^r + I_2^r \cos(2\psi)\} \hat{i} \\ \{I_2^r \sin(2\psi)\} \hat{j} \\ \{-i2 I_1^r \cos(\psi)\} \hat{k} \end{bmatrix}$$

where once again we have

$$I_0^r = \int_0^{\min(\theta_{max}, \theta_c)} E_{inc}(\theta) \sqrt{\cos \theta} (R_s^{(1,j)} - R_p^{(1,j)} \cos \theta_j) J_0(k_1 \rho \sin \theta) e^{-ik_j z \cos \theta_j} \sin \theta d\theta$$

$$I_1^r = \int_0^{\min(\theta_{max}, \theta_c)} E_{inc}(\theta) \sqrt{\cos \theta} R_p^{(1,j)} \sin \theta_k J_1(k_1 \rho \sin \theta) e^{-ik_j z \cos \theta_j} \sin \theta_1 d\theta$$

$$I_2^r = \int_0^{\min(\theta_{max}, \theta_c)} E_{inc}(\theta) \sqrt{\cos \theta} (R_s^{(1,j)} + R_p^{(1,j)} \cos \theta_j) J_2(k_1 \rho \sin \theta) e^{-ik_j z \cos \theta_j} \sin \theta d\theta \quad (12)$$

Note that in all subsequent simulations we have used $n = 3$.

IV. RESULTS AND DISCUSSIONS

A. SIMULATIONS

A computer simulation was developed using Eqns. 8 and 12 to determine the electric field inside our sample chamber. As per specifications, the Zeiss objective focal length was taken to be 1.8 mm or 1800 μm , and the numerical aperture (NA) 1.41. The wavelength of light was 1.064 μm , while the velocity of light in vacuum was considered to be 1. The beam waist after the objective was assumed to be 0.5 μm , which we obtained by measuring the beam waist after our trapping objective. This is consistent with the minimum obtainable theoretical resolution corresponding to $\frac{\lambda}{2NA}$, λ and NA for our experiment being 1064 nm and 1.41 respectively. We also considered only propagating light waves and not the evanescent components. This is consistent with our experimental observation of not obtaining any ring formation near the cover slip, a fact that rules out any evanescent coupling with the microspheres.

The model was verified for the field intensity distribution around the focus of a high numerical aperture lens and produced the well known Airy fringes at the beam focus. The

field distribution also showed a slight asymmetry or elongation around the direction of polarization of the light beam as expected. However, only Airy fringes are not sufficient to trap particles away from the center since the power in these fringes is very low compared to that in the central maxima. Next, we considered an aplanatic lens focusing into a single interface (glass/water). Again as expected, we saw signatures of spherical aberration, with the focal spot shifting from the geometric focus, and more importantly, some power being redistributed in the form of side lobes in the beam. Note that for both these cases, only Eqns. 8 were used since there was no reflected component of the field.

Finally, we considered three interfaces akin to our experimental sample chamber in Configuration 1. After the microscope objective, the three interfaces are: 1) index-matching microscope objective oil and cover slip (English glass or polymer), 2) cover slip and sample (water), 3) water and top slide (glass). To determine the effect of the 160 and 250 μm coverslips in the radial distribution of the field for sample thicknesses used in our experiment, we did not consider a third interface. These results are shown in Figs. 5 and 6. In Fig. 7, we show the results for all three interfaces, including the top glass slide. The thickness of the sample (water layer) for all simulations was 30 μm , the same as the experimental value used. The geometric focus was placed 15 μm inside the water layer in each case, the distance being measured from the coverslip-water interface. Only the results for the transmitted field are given. In Fig. 7, the field inside the chamber was calculated by a superposition of Eqns. 8 and 12, while for Fig. 5 and 6, only Eqn. 8 was used.

B. ANALYSIS

Fig. 5 shows the results for the field profile in the xz plane obtained for 160 and 250 μm coverslips. Both plots show considerable aberrations, which results in the distortion of the focal spot and distributes more power to the side lobes. For 160 μm coverslips, as shown in Fig. 6a, the focal spot has shifted towards the negative z -direction, i.e. towards the coverslip, and is now at around 13 μm (a change of -2 μm) inside the water layer of the sample chamber. The plot clearly shows the side lobes that arise in the backward direction due to excess aberration. In contrast, for 250 μm coverslips as shown in Fig. 6a, the focus has shifted in a direction opposite to that obtained in the former case, i.e. in the positive z -direction, and the amount of shift is around 5 μm . The plot clearly shows the side lobes

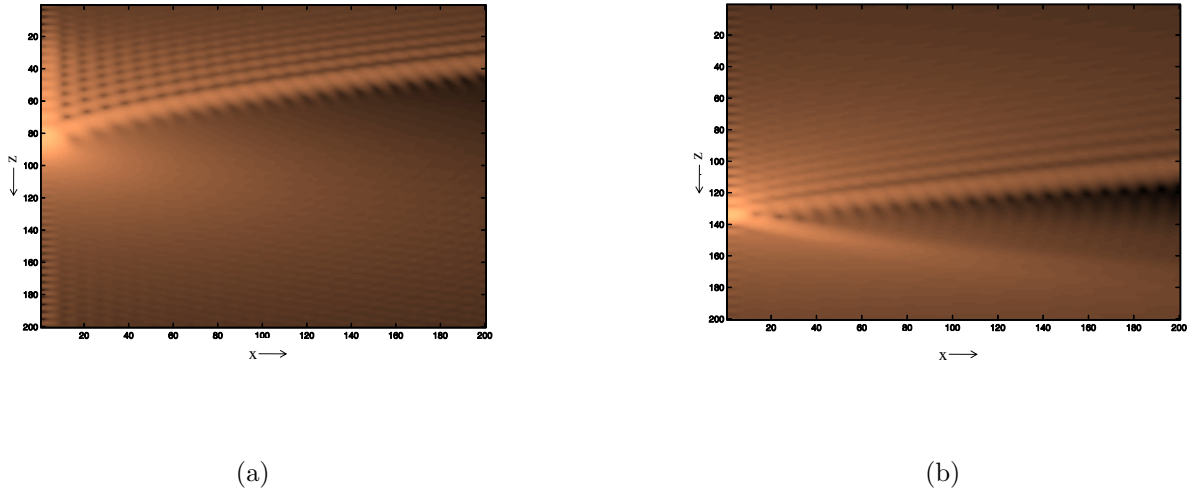


FIG. 5: XZ intensity plot for (a) 160 μm coverslip, and (b) 250 μm coverslip ($0 < x < 10 \mu\text{m}, -15 < z < 15 \mu\text{m}.$) in Configuration 1. The trapping beam propagates along the z -direction. Both plots show distortions of the focal spots with power being redistributed into side lobes. In (a), the focal spot has shifted in the negative z -direction and side lobes arise in the backward direction with respect to beam propagation, while in (b), the focal spot has shifted in the positive z -direction and side lobes arise in the forward direction with respect to beam propagation.

that arise in this case in the backward direction due to excess aberration.

A crucial difference between the side lobes developed for the two types of cover slips is that for the 160 μm case, the power in the side lobes *never* exceeds the power in the central lobe. This has been tested out by taking xy cross-sections of the field at various distances from the actual focus for both 160 and 250 μm coverslips. The xy cross-sections at a distance 4 μm from the focus (considered since we observe the rings at a distance of around 24 μm inside the sample chamber) for both types of coverslips have been shown in Fig. 6. For 160 μm coverslips, the maximum intensity we obtain at the laser focus is around .036 (normalized with respect to incident beam maximum intensity taken as 1) from Fig. 6a. Another interesting observation is that the maxima of the side lobes occur at a different axial position from the maxima of the central lobe - something that has important consequences in imaging particles that could be trapped in these lobes.

The situation is different for the 250 μm coverslips. As shown in Fig. 5b, although the peak intensities are lower than those corresponding to the 160 μm case (thus causing lower trap stiffness in this case), the refractive index mismatch has resulted in more power from the central lobe being distributed into the side lobes. This could then facilitate the formation of the particle rings for the 250 μm case. Also, the maximum intensity in the side lobe is around .0038, about a factor of 9.5 lower than for 160 μm coverslips. Since trapping force is directly proportional to light intensity, this signifies a similar ratio for the force between glass and polymer coverslips. This is a direct vindication of our measurements of corner frequency reported in Section II for beads trapped in the center for 160 μm coverslips and in the side lobes for 250 μm coverslips. Another crucial point to note is the distance of the side lobe maximum from the center (that would correspond to the ring radius), which from Fig. 6b is around 2.3 μm . This fits very well indeed with the experimentally observed diameters of around 4 - 5 μm for the particle rings. Also, if the beam waist is increased from 0.5 μm to around 1 μm , the side lobe maximum comes nearer to the center for the same xy plane we consider (i.e. 4 μm away from the focus) as in the former case. This explains our experimental observation that for small input beam diameters (for which the beam waist would be larger), the ring diameter is also small.

However, the radial fringes are still not enough to support axial trapping, as is evident from our experimental findings where we do not obtain ring structures with just the sample on a coverslip. This tells us that there is still a need to accentuate axial trapping for achieving stable trapping in a ring. The enhanced axial trapping is provided by the top slide. Enhanced axial trapping due to the presence of a reflective surface has been studied in Ref. 20. That study dealt with a similar set-up such as ours with a trapping chamber consisting of the sample sandwiched between coverslip and a top slide. It was shown that the top and bottom surface form a standing wave cavity with interference fringes formed by superposition of the transmitted trapping light and that reflected from the top slide of the sample chamber causing alternate regions of stable axial trapping near the slide. The authors calculated the nodes of the trapping force developed near the top slide and experimentally showed trapped particles hopping between different stable equilibrium axial positions. However, they did not consider the radial component of the trapping field in their theoretical calculations, and did not experimentally observe any confinement away from the trap center. The enhanced spherical aberration in our system provides the radial confinement, while the

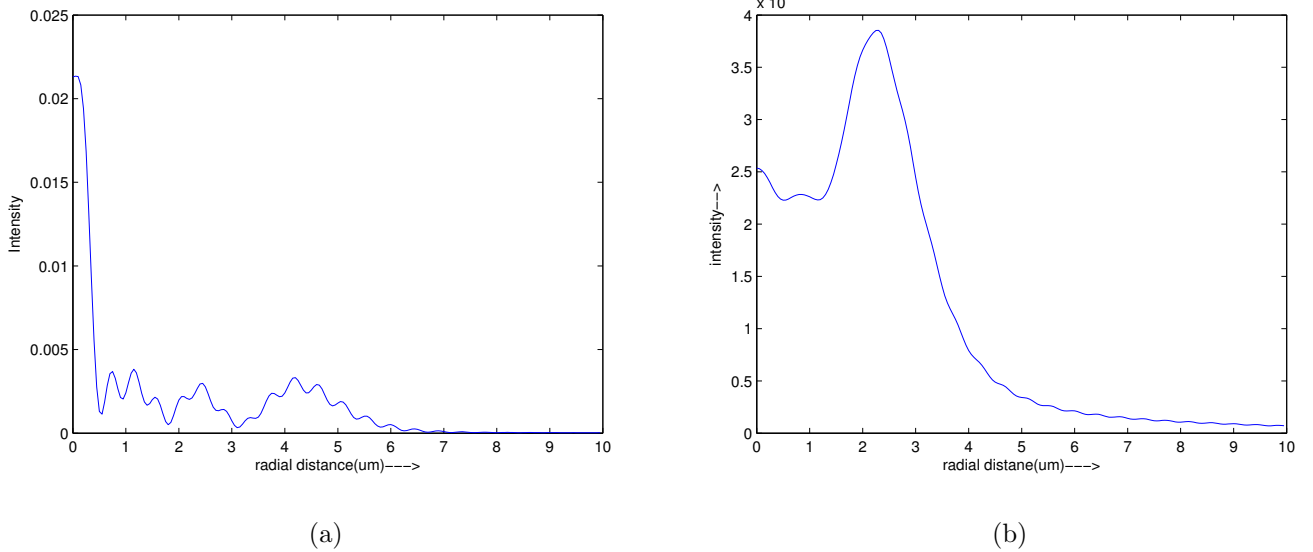
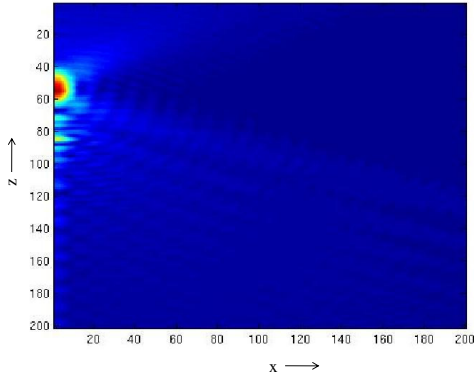


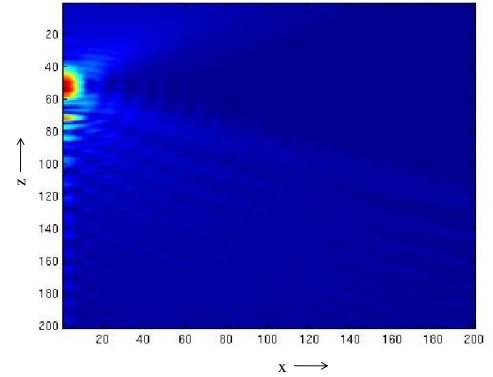
FIG. 6: Radial intensity plot at a plane $4\mu\text{m}$ away from focus for (a) $160\mu\text{m}$ coverslip, (b) $250\mu\text{m}$ coverslip in Configuration 1. In (a), the power in the central lobe is much higher than the side lobe, while in (b), the power in the side lobe is higher than in the central lobe. The total power in the central lobe (0.036 in normalized units) for (a) is, however, higher than that in the side lobe for (b) (0.0038).

top slide stabilized the trap axially. To investigate this by a simulation, we consider a four layered media now, with the fourth media representing the glass slide having a refractive index of 1.516. The top slide contributes to reflected waves that causes additional axial fringes to develop within the electric field distribution as shown in the xz plots in Figure 7. The location and separation of the fringes depends on the thickness of the water layer and also on the position of the focus with respect to the top glass slide - water interface. The figures were generated with focal spot $6\mu\text{m}$ below the glass slide water interface. However, the depth of the water layer was $28\mu\text{m}$ in Figure 7a and $35\mu\text{m}$ in Figure 7b. The variation in location of the axial fringes is apparent in both plots.

It is also clear why the rings are observed only when the beam focus is close to the top glass slide. As is apparent from our simulations shown in Fig. 7, as well as in the results given in Ref. 20, the axial fringes are located near the top slide only and die away very fast as one goes farther into the sample solution. This is intuitively understandable considering the fact that we are working with very fast diverging Gaussian beams in this case, and a



(a) Axial fringes: water thickness $28 \mu\text{m}$



(b) Axial fringes: water thickness $35 \mu\text{m}$

FIG. 7: Axial fringes produced due to reflections from top slide at different sample thicknesses ($0 < x < 10 \mu\text{m}, -15\text{m} < z < 15 \mu\text{m}$).

constructive superposition could be achieved only when the incident beam and reflective surface are very close. This also explains why we did not observe the patterns at sample thicknesses of more than around $30 \mu\text{m}$. For greater distances, we could not get the beam focus close enough to the top slide to facilitate axial trapping, as a result of which the ring structures were not axially stable.

We need also mention that such ring formation has also been observed with the $160 \mu\text{m}$ coverslips, but only when the imaging was done external to the microscope. This could be understood from the fact that the imaging system of our microscope is optimized in the case of $160 \mu\text{m}$ coverslips to image the focal plane, and since we observe from our simulations that the side lobes are axially slightly shifted away from the focus - one needs to develop a separate imaging system with lenses in order to observe the axially shifted side lobes where particles are trapped radially. This is not the case for $250 \mu\text{m}$ coverslips, where the enhanced spherical aberration affects the imaging as well, and one can image the side lobes even with the imaging camera at the microscope side port itself (note that in this case, the side lobes are axially shifted even more from the central lobe).

V. CONCLUSIONS

The self-assembly we observe could be used for several interesting applications, the most obvious being the study of optical binding. This is the phenomenon where the equilibrium position of a trapped microparticle is modified due to the presence of a second trapped particle in its vicinity [10]. The electric field due to one microparticle, which is actually an induced dipole, alters the electric field perceived by the other, and therefore alters its equilibrium position. Optical binding could significantly affect the dynamics of such self assembly - something that could be studied by a theoretical model and even verified experimentally if one could continuously monitor the corner frequency of a trapped microparticle and study how it gets modified due to the entry of other particles into the trap. The measurement could be performed by a high speed camera or even by a standard position detector such as a quadrant photodiode. We have observed instances of optical binding in our patterns, especially when there are a small number of particles - the particles seem to favour equilibrium positions that are slightly far away from each other due to the effects of optical binding. Thus, direct measurements of optical binding could be facilitated by such structures.

The fact that we are able to trap particles at the center as well in the sides, as has been shown in Fig. 2, facilitates another interesting experiment - that of observing Kramer's transitions or thermally driven transitions that occur due to stochastic fluctuations in the amplitude of the Brownian motion of the trapped particle [21]. These have been typically observed in a dual optical trap where a particle hopped between traps with transition rates depending on the trap potential depth and separation. Our trapping arrangement with enhanced spherical aberration automatically renders such a potential pair possible even with a single trapping beam, and we have indeed observed hopping in our experiments, where a particle in the center has suddenly jumped to the outer ring, and vice versa. We plan careful studies of these transitions in future experiments.

The ring pattern can be of use in biological applications as well, with the possibility of studying controllable cell to cell interactions, such as that between cancer cells and Natural Killer cells [9]. Also, the possibility of applying differential force in the center and the sides of a single trapped cell could facilitate measurements of cell elasticity, where the cell is stretched and then unstretched by switching off the trap momentarily (which may be accomplished by modulating the trap by an acousto-optic modulator).

Future work would revolve around the applications mentioned above. However, one of the immediate things we are working on is the calculation of the forces in the axial and radial directions by using the Generalized Lorentz Mie theory [22]. While the intensity calculations shown in this paper give us a clear understanding of the phenomenon we report, a detailed force calculation would also give more quantitative understanding and also identify the stable positions where particles could be trapped in the axial and radial directions in the trapping chamber in an optical trap.

In conclusion, we have shown spontaneous assembly of $1.1\ \mu\text{m}$ particles in a ring formation for single beam optical tweezers without the use of spatially manicured optical beams or holographic patterns coupled into the optical trap. The patterns are observed in a standard trapping chamber consisting of a coverslip stuck to a top slide with the sample consisting of the particles immersed in water solution sandwiched between them. The patterns are seen for the normal imaging configuration of the trapping assembly with the camera attached to the microscope side port only when we use polymer coverslips that are thicker and have higher refractive index than glass coverslips typically used for optical trapping. This is due to the fact that spherical aberration comes into play because of the mismatch of the refractive indices between the immersion oil, coverslip and water in which the beads were suspended. The net spherical aberration is able to elongate the focal spot axially and divert more power to the side fringes, and increase the chances of ring formation. However, a distinction between the power distribution in the side fringes and the central maxima is seen between the $250\ \mu\text{m}$ and $160\ \mu\text{m}$ coverslips respectively. The aberration in the case of $250\ \mu\text{m}$ is much higher compared to that in the $160\ \mu\text{m}$ case, since the refractive index of the $250\ \mu\text{m}$ coverslip is significantly different from the immersion oil refractive index. This additional aberration is responsible for creating regions in the sample chamber where the intensity of the radial side fringes is more than that in the central lobe in that plane. This could in principle then provide an explanation as to why radial trapping is seen easily in the case of $250\ \mu\text{m}$ coverslips. The axial trapping is provided by top glass slide. The reflected light from the glass slide produces axial interference fringes on the radial fringes existing already, which in turn creates pockets of high intensity such that the trapping of the micro-spheres gets axially stabilized within the rings. We believe that this kind of assembly formation due to only optical effects is quite novel and has not been observed before. We envisage several applications for this assembly, including optical binding, study of thermally

driven transitions, and biological interactions.

VI. ACKNOWLEDGEMENTS

This work was supported by the Indian Institute of Science Education and Research, Kolkata, an autonomous research and teaching institute funded by the Ministry of Human Resource Development, Govt. of India. The authors would also like to acknowledge Dr. Kaushik Biswas and Dr. Basudeb Karmakar of CGCRI Kolkata, for help in measuring the refractive indices of the glass and polymer coverslips.

-
- [1] L. P. Ghislain, N. A. Switz, and W. W. Webb, *Rev. Sci. Instrum.*, **65**, 2762 (1994).
 - [2] G. Volpe and D. Petrov, *Phys. Rev. Lett.*, **97**, 210603 (2006).
 - [3] A. R. Clapp, A. G. Ruta, and R. B. Dickinson, *Rev. Sci. Instrum.*, **70**, 26 (1999).
 - [4] K. Svoboda, C. F. Schmidt, B. J. Schnapp, and S. M. Block, *Nature*, **365**, 721 (1993).
 - [5] A. D. Mehta, M. Rief, J. A. Spudich, D. A. Smith, and R. M. Simmons, *Science*, **283**, 1689 (1999).
 - [6] D. E. Smith, S. J. Tans, S. B. Smith, S. Grimes, D. L. Anderson, and C. Bustamante, *Nature (London)*, **413**, 748 (2001).
 - [7] J.-D. Wen, M. Manosas, P. T. X. Li, S. B. Smith, C. Bustamante, F. Ritort, and I. Tinoco, *Biophys. J.*, **92**, 2996 (2007).
 - [8] C. Hosokawa, H. Yoshikawa, and H. Masuhara, *Phys. Rev. E*, **72**, 021408 (2005).
 - [9] R. Oldham, *Cancer Metastasis Rev.*, **2**, 323 (1983).
 - [10] K. Dholakia and P. Zemanek, *Rev. Mod. Phys.*, **82**, 595 (2010).
 - [11] M. Padgett and R. Bowman, *Nature Photon.*, **5**, 343 (2011).
 - [12] H. B. W. G. Lee and J. K. Chang, *Curr. Appl. Phys.*, **6S1**, e237 ((2006)).
 - [13] S. Ahlawat, R. Dasgupta, and P. K. Gupta, *J. Opt. A: Pure Appl. Opt*, **9**, S189 ((2007)).
 - [14] K. Berg-Sorensen and H. Flyvbjerg, *Rev. Sci. Inst.*, **75** (2004).
 - [15] K. C. Neuman and S. M. Block, *Rev. of Sci. Inst.*, **75** (2004).
 - [16] C. J. R. Sheppard and M. Gu, *Opt. Comm.*, **41**, 180 (1992).

- [17] A. A. R. Neves, A. Fontes, C. L. Cesar, A. Camposeo, R. Cingolani, and D. Pisignano, *Phys. Rev. E*, **76**, 061917 ((2007)).
- [18] M. Born and E. Wolf, *Principles of Optics* (Pergamon Press, 1989).
- [19] A. Rohrbach, *Phys. Rev. Lett.*, **95**, 168102 (2005).
- [20] P. Zemnek, A. Jons, and E.-L. Florin, *Opt. Lett.*, **26**, 1466 (2001).
- [21] L. I. McCann, M. Dykman, and B. Golding, *Nature*, **402**, 785 (1999).
- [22] N. Malagnino, G. Pescea, A. Sasso, and E. Arimondo, *Opt. Comm.*, **214**, 15 (2002).
- [23] Y. Zhang, C. Gu, A. M. Schwartzberg, S. Chen, and J. Z. Zhang, *Phys. Rev. B*, **73**, 165405 (2006).
- [24] D. Grier, *Nature*, **424**, 810 (2003).